1.6-Gb/s 16-Level Superposed APSK Modem with Baseband Signal-Processing Coherent Demodulator

MAKOTO WASHIO, TADAO SHIMAMURA, MEMBER, IEEE, NORIO KOMIYAMA, AND YUKIO TAKIMOTO

Abstract—**A 1.6-Gb/s 16-level superposed APSK modem using a newly developed baseband signal-processing coherent demodulator is described. In the modulator, the superposing modulation method is adopted in which two QPSK carriers having different levels are superposed so that the combined signal forms a 16-level APSK carrier. Sixteen signal points are arranged in lattice form on the signal space. In the demodulator, a newly developed carrier recovery loop is adopted in which quantizing error signals are detected in the process of data regeneration; they are used for generating the phase error signal to control a VCO. The principles of operation and theoretical analysis of this carrier recovery loop is described, through which it is shown that the recovered carrier has inherently low-pattern jitter power. Furthermore, it features a very simple circuit configuration. The circuit configurations of an experimental modem and some important test results are described in detail. It is shown that the modem has improved performance characteristics in such a high-speed region as 1.6 Gb/s while its circuit configuration is much simplified.**

I. Introduction

MULTIPLE amplitude and phase shift keying (MAPSK) [1]–[6] is considered to be an advantageous means for effective use of the transmission frequency band, and the feasibility of realizing an MAPSK modem for use in microwave digital transmission systems has been studied recently [3]–[5]. Among these the 16-level APSK system in which signal points are arranged in a lattice form on the signal space has attracted particular attention because of its high transmission efficiency and realizability.

Although the MAPSK system has the advantage of effective use of signal space, it has the disadvantage of being subject to degradations ascribable to various distortions caused in the transmission path and imperfections in the modulator and demodulator. Of the imperfections in the modulator and demodulator, the phase and amplitude deviation of the modulated carrier, distortions caused in the signal processing system in the demodulator, and static phase error and jitter of the recovered reference carrier are dominant.

Manuscript received May 31, 1978.

M. Washio is with Yokosuka Electrical Communication Laboratory, 1-2356 Take, Yokosuka, 238-03 Japan.

T. Shimamura, N. Komiyama, and Y. Takimoto are with the Millimeter Wave Communication Development Department, 4035 Ikebe-Cho, Midori-Ku, Yokohama 226, Japan.

These distortions tend to give much more degradation to the transmission quality than in conventional two- or four-phase PSK systems.

Accordingly, in order to realize a MAPSK modem, it is required, first of all, to minimize distortions in the modulation and demodulation process and to realize such a carrier recovery circuit that gives extremely small stationary phase error and pattern jitter. Needless to say, these requirements become more difficult to be satisfied as the modulation speed becomes higher.

Ishio *et al.* [3] have proposed the superposed modulation–demodulation method as a means for realizing high-speed and high-performance 16-level APSK transmission, and one of the authors has reported experimental studies of a 1.6-Gb/s APSK modem and verified its feasibility [4], [9].

Following the efforts above mentioned, a new 16-level APSK modem based on different principles of operation in the demodulator has been devised. The modem features a simple-construction high-speed operation, and high immunity against transmission distortions while having better performances. Its excellent performance has been verified both theoretically and experimentally.

In this paper, the configuration of the modem, the principles of operation of the newly devised demodulator, and the performance of the engineering model for a 400-MB 16-level (1.6-Gb/s) APSK signal will be described.

II. Principles of Modulation and Demodulation

A. Modulation

In the modulator, the superposed modulation is adopted, which is shown in Fig. 1.

A 16-level APSK signal is obtained by superposing a four-phase PSK signal on another four-phase PSK signal, by giving a proper amplitude ratio and phase relationship to these signals. These signals are called the first-path signal $S_1(t)$ and the second-path signal $S_2(t)$, respectively. By selecting the second-path signal level to be 6 dB lower than the first-path signal level, 16 symbols represented by four binary data signals are arranged in a lattice form on a two-dimensional signal space. This relationship is shown

0018-9480/78/1200-0945$00.75 ©1978 IEEE

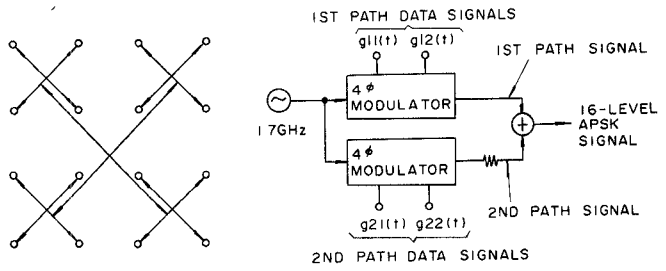

Fig. 1. Superposed APSK modulator. (a) Signal constellation. (b) Block diagram.

in Fig. 1. The 16-level APSK signal $S(t)$ can be given by

$$S(t) \triangleq S_1(t)+S_2(t)$$
$$=\left\{\sqrt{2}\, g_{11}(t)\cos\omega_c t+\sqrt{2}\, g_{12}(t)\sin\omega_c t\right\}$$
$$+\left\{\frac{\sqrt{2}}{2} g_{21}(t)\cos\omega_c t+\frac{\sqrt{2}}{2} g_{22}(t)\sin\omega_c t\right\} \quad (1)$$

where ω_c denotes the angular frequency of the carrier, and $g_{ij}(t)$ the binary data signals given by

$$g_{ij}(t)=\sum_k a_{ij}(t+kT), \qquad a_{ij}(t)=\begin{cases} +1 \\ \text{or,} \\ -1 \end{cases} \quad -\frac{T}{2}\leqslant t\leqslant\frac{T}{2}$$
$$0, \qquad |t|>\frac{T}{2}$$

and $1/T$ denotes the symbol rate.

As stated above, this modulation scheme has an advantage in that the highly accurate modulated carrier can be easily obtained because each four-phase PSK signal can be obtained in high accuracy by established techniques.

B. Demodulation

In a 16-level APSK system, signals are arranged more densely in the signal space than in the four-phase PSK modulation; accordingly, in a demodulation system, it is necessary to avoid the distortion in signal processing and to realize an accurate data regeneration. This condition requires the circuit configuration to be as simple as possible. It is also necessary to reduce the stationary phase error and the phase jitter of the reference carrier for coherent detection to an extremely small value.

The demodulation system proposed in this paper was devised considering the above conditions. The system is based on the decision feedback scheme [7], [8] which comprises the feed-forward quantizer for data regeneration and the carrier recovery loop utilizing the quantization error and the regenerated data to produce the phase error signal.

Fig. 2 shows the schematic diagram of this demodulation system. The input modulated carrier is demodulated to baseband signals in two phase detectors using two reference carriers which are orthogonal to each other. These two baseband signals are referred to as the I-channel signal and Q-channel signal, respectively. Each demodulated baseband signal is quantized into two bits of data signal by a feed-forward quantizer which consists of two stages of unit quantizers. The unit quantizer comprises a decision circuit, a low-pass filter, and a subtractor. The output of the first subtractor is fed to the second quantizer. The regenerated data signals are obtained from the decision circuits. The outputs of the second subtractors and the first decision circuits in both signal paths are used to generate the phase error signal by the signal processing scheme shown in the figure.

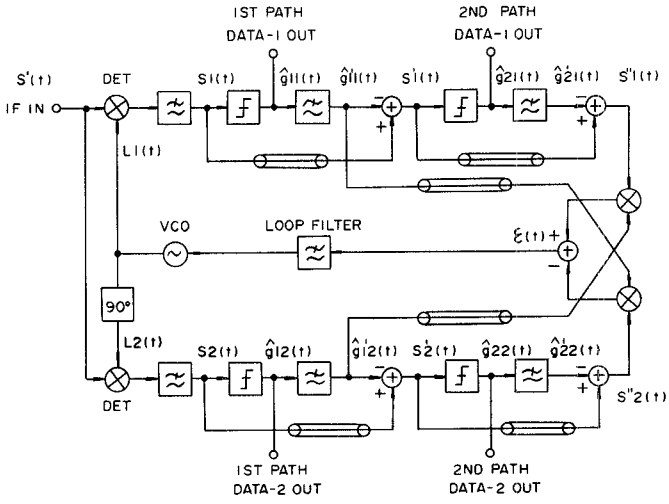

Fig. 2. Block diagram of demodulator.

The above mentioned scheme and important characteristics for the data regeneration and the carrier recovery are shown below analytically.

Suppose, for simplicity, that the amplitude and delay frequency characteristics of the transmission path are symmetrical about the carrier frequency ω_c, and the transfer function and impulse response of its equivalent low-pass filter are $H(j\omega)$ and $h(t)$, respectively. Then the receiving input signal to the demodulator $S'(t)$ can be given by

$$S'(t)=\sqrt{2}\left\{g'_{11}(t)+\frac{1}{2}g'_{21}(t)\right\}\cos\omega_c t$$
$$+\sqrt{2}\left\{g'_{12}(t)+\frac{1}{2}g'_{22}(t)\right\}\sin\omega_c t+n(t) \quad (2)$$

where

$$g'_{ij}(t)=\int_{-\infty}^{\infty} g_{ij}(\tau)h(t-\tau)d\tau$$

and $n(t)$ denotes the white Gaussian noise.

The reference carriers for coherent demodulation $L_1(t)$ and $L_2(t)$, can be expressed by

$$L_1(t)=\sqrt{2}\cos(\omega_c t+\phi_e)$$
$$L_2(t)=\sqrt{2}\sin(\omega_c t+\phi_e) \quad (3)$$

where ϕ_e denotes the phase error of the reference carrier.

From (2) and (3), the phase detector outputs $s_1(t)$ and $s_2(t)$ can be expressed by

$$s_1(t) \triangleq [S'(t)\times L_1(t)]_l$$
$$= \left\{ g'_{11}(t)+\frac{1}{2}g'_{21}(t)\right\}\cos\phi_e$$
$$-\left\{ g'_{12}(t)+\frac{1}{2}g'_{22}(t)\right\}\sin\phi_e + n_I(t)$$
$$s_2(t) \triangleq [S'(t)\times L_2(t)]_l$$
$$= \left\{ g'_{11}(t)+\frac{1}{2}g'_{21}(t)\right\}\sin\phi_e$$
$$+\left\{ g'_{12}(t)+\frac{1}{2}g'_{22}(t)\right\}\cos\phi_e + n_Q(t) \quad (4)$$

where $[\ ]_l$ denotes the low-frequency component of $[\ ]$ and $n_I(t)$ and $n_Q(t)$ denote the in-phase and quadrature component of the noise, respectively. The effect of the noise added in the transmission path is neglected in the following analysis because this will give a negligible effect on the performance of the demodulator.

If $\phi_e \ll 1$, we have from (4)

$$s_1(t) \cong \left\{ g'_{11}(t)+\frac{1}{2}g'_{21}(t)\right\}\cos\phi_e$$

and

$$s_2(t) \cong \left\{ g'_{12}(t)+\frac{1}{2}g'_{22}(t)\right\}\cos\phi_e.$$

Then, the polarity discriminated signals $\hat{g}_{11}(t)$ and $\hat{g}_{12}(t)$ are given by

$$\hat{g}_{11}(t)=g_{11}(t) \quad \hat{g}_{12}(t)=g_{12}(t). \quad (5)$$

Thus the data signals of the first path are regenerated.

The outputs signals $\hat{g}'_{11}(t)$ and $\hat{g}'_{12}(t)$ of the low-pass filters which have the equivalent low-pass characteristic to the transmission path are equal to $g'_{11}(t)$ and $g'_{12}(t)$, respectively, from (2) and (5). Then, we can obtain the first quantizing error signals $s'_1(t)$ and $s'_2(t)$ as follows:

$$s'_1(t) \triangleq s_1(t)-\hat{g}'_{11}(t)$$
$$= g'_{11}(t)(\cos\phi_e-1)+\frac{1}{2}g'_{21}(t)\cos\phi_e$$
$$-\left\{ g'_{12}(t)+\frac{1}{2}g'_{22}(t)\right\}\sin\phi_e$$
$$s'_2(t) \triangleq s_2(t)-\hat{g}'_{12}(t)$$
$$= g'_{12}(t)(\cos\phi_e-1)+\frac{1}{2}g'_{22}(t)\cos\phi_e$$
$$-\left\{ g'_{11}(t)+\frac{1}{2}g'_{21}(t)\right\}\sin\phi_e. \quad (6)$$

In the second quantizer in each route, the signal processing is conducted in the same way as the first quantizer so that, if $\phi_e \ll 1$, the polarity discriminated signals $\hat{g}_{21}(t)$ and $\hat{g}_{22}(t)$ and the second quantizing error signals are given by (7) and (8), respectively.

$$\hat{g}_{21}(t)=g_{21}(t) \quad \hat{g}_{22}(t)=g_{22}(t) \quad (7)$$
$$s''_1(t) \triangleq s'_1(t)-\frac{1}{2}\hat{g}'_{21}(t)$$
$$= \left\{ g'_{11}(t)+\frac{1}{2}g'_{21}(t)\right\}(\cos\phi_e-1)$$
$$-\left\{ g'_{12}(t)+\frac{1}{2}g'_{22}(t)\right\}\sin\phi_e$$
$$s''_2(t) \triangleq s'_2(t)-\frac{1}{2}\hat{g}'_{22}(t)$$
$$= \left\{ g'_{12}(t)+\frac{1}{2}g'_{22}(t)\right\}(\cos\phi_e-1)$$
$$-\left\{ g'_{11}(t)+\frac{1}{2}g'_{21}(t)\right\}\sin\phi_e. \quad (8)$$

Following the signal processing scheme shown in Fig. 2, the phase error signal $\epsilon(t,\phi_e)$ can be obtained as follows:

$$\epsilon(t,\phi_e) \triangleq s''_1(t)\cdot\hat{g}'_{12}(t)-s''_2(t)\cdot\hat{g}'_{11}(t)$$
$$= -\{g'^2_{11}(t)+g'^2_{12}(t)\}\sin\phi_e-\frac{1}{2}\{g'_{11}(t)$$
$$\cdot g'_{22}(t)+g'_{12}(t)\cdot g'_{21}(t)\}$$
$$\cdot\sin\phi_e-\frac{1}{2}\{g'_{12}(t)\cdot g'_{21}(t)-g'_{11}(t)\cdot g'_{22}(t)\}$$
$$\cdot(\cos\phi_e-1). \quad (9)$$

If $g_{ij}(t)$'s $(i,j:1,2)$ are the stochastic processes which are zero (0) in average and statistically independent to each other, then

$$\bar{\epsilon}(t,\phi_e) = -K\sin\phi_e \quad (10)$$

where

$$K=\overline{\{g'^2_{11}(t)+g'^2_{12}(t)\}}.$$

If there is no band limitation in the transmission path, we have, from (1), $K=2$.

So far, we have analyzed the operation in the neighborhood of $\phi_e=0$. Likewise, we can easily obtain $\bar{\epsilon}(t,\phi_e)$ in the neighborhood of $\phi_e=(2\pi/4)\cdot k$ $(k=0,1,2,3)$ as follows:

$$\bar{\epsilon}(t,\phi_e) = -K\sin\left(\phi_e-\frac{2\pi}{4}k\right). \quad (11)$$

That is, the time average of $\bar{\epsilon}(t,\phi_e)$ is nearly proportional to the phase error ϕ_e in the neighborhood of $(2\pi/4)k$ $(k=0,1,2,3)$.

The equivalent phase comparator characteristic $\bar{\epsilon}(t,\phi_e)$ calculated by a computer for a range of $|\phi_e| \leqslant \pm\pi/4$ is shown in Fig. 3. It is to be noted that the phase error signal $\epsilon(t,\phi_e)$ given by (9) involves only an extremely small amount of noise component. This is explained as follows. The second and third terms of (9) are noise components depending on the pattern of the modulated data signal. When $\phi_e \ll 1$, the third term of (9) can be neglected. Then

$$\epsilon(t,\phi_e) \simeq -\{g'^2_{11}(t)+g'^2_{12}(t)\}\phi_e$$
$$-\tfrac{1}{2}\{g'_{11}(t)\cdot g'_{22}(t)+g'_{12}(t)\cdot g'_{21}(t)\}\phi_e \quad (12)$$

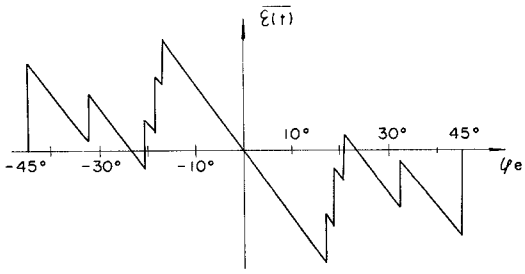

Fig. 3. Equivalent phase detector characteristic of carrier recovery loop.

That is, the noise component of $\epsilon(t,\phi_e)$ is reduced in proportion to ϕ_e.

The signal-to-noise ratio of the recovered carrier can be estimated by calculating the power spectrum of $\epsilon(t,\phi_e)$ from (10) and integrating it over the noise bandwidth of the phase lock loop. Suppose the transmission path has no band limitation for simplicity, then, from (1) and (9),

$$\epsilon(t,\phi_e) = -2\phi_e - \tfrac{1}{2}\epsilon'(t)\cdot\phi_e \tag{13}$$

where

$$\epsilon'(t) \triangleq g_{11}(t)\cdot g_{22}(t) + g_{12}(t)\cdot g_{21}(t).$$

The autocorrelation function of $\epsilon'(t)$, $\varphi(\tau)$ is given by

$$\varphi(\tau) = 1 - \left|\frac{\tau}{T}\right|, \qquad -T \leqslant t \leqslant T$$
$$= 0, \qquad T > |t| \tag{14}$$

and the power frequency spectrum of $\epsilon'(t)$, $S'(j\omega)$ is given by

$$S'(j\omega) = F\{\varphi(\tau)\} = \frac{T}{2\pi}\cdot\left[\frac{\sin\frac{\omega T}{2}}{\frac{\omega T}{2}}\right]^2 \tag{15}$$

where $F\{\cdot\}$ denotes a Fourier integral.

Thus, if the frequency response of the loop is $H_l(j\omega)$, the noise power N included in the recovered carrier is given by

$$N = \phi_e\int_{-\infty}^{\infty} N_0\cdot\frac{T}{2\pi}\cdot\left[\frac{\sin\frac{\omega T}{2}}{\frac{\omega T}{2}}\right]^2\cdot|H_l(Sj\omega)|^2 d\omega$$
$$\simeq N_0 T B_l \phi_e/2\pi, \qquad \text{if} \quad TB_l \ll 1 \tag{16}$$

where

$$N_0 \triangleq \overline{\left\{\frac{1}{4}\epsilon'(t)\right\}^2} = \frac{1}{8} \qquad \text{and} \qquad B_l = \int_{-\infty}^{\infty}|H_l(j\omega)|^2 d\omega.$$

Hence, we have

$$S/N \simeq 10\log\left(\frac{TB_l\phi_e}{16\pi}\right)^{-1}, \qquad \text{dB}. \tag{17}$$

As shown above, the signal-to-noise ratio can be made extremely large, in principle, by this carrier recovery loop.

It is to be noted, regarding the equivalent phase comparator characteristic shown in Fig. 3, that undesired stable points exist at about $\pm 21°$. However, these points will not substantially be stable points because a little noise included in the input carrier causes the characteristic curve not to cross the abscissa at the subject points. Accordingly, there may be no false lock phenomenon. This is verified by the experimental data given later in this paper.

It has been clarified through the above discussion that this method substantially provides various advantages, namely, 1) a recovered carrier having very small pattern jitter, and no false lock phenomenon, 2) a simple circuit configuration, and 3) a capacity for high-speed operation.

III. Performance of Experimental Modem

A 16-level APSK modem based on the principles of operation described in the preceding section has been implemented for experimental purpose, of which the transmission capacity is 1.6 Gb/s. Table I gives the major design parameters and characteristics of the modem. The circuit configuration and the performances of the modem will be described in this section.

A. Modulator

The modulator is composed of two four-phase PSK modulators as shown in Fig. 1. Each modulator is composed of two ring modulators. The IF frequency and symbol rate are 1.7 GHz and 400 MHz, respectively.

The major characteristics of each four-phase modulator are as follows. The modulation phase error is within $\pm 1.5°$; the modulation amplitude deviation is within ± 0.2 dB; the rise time is less than 0.7 ns; and the pulsewidth variation is ± 75 ps. Fig. 4 shows the signal constellation of the superposed APSK signal measured by a network analyzer, which shows that an extremely high accuracy signal arrangement is achieved. The pulsewidth variation of the modulated carrier is less than ± 100 ps.

B. Demodulator

The double balanced mixer is used as the coherent detector for demodulation, which has substantially the same configuration as the ring modulator used in the modulator. The detector has a wide-band characteristic over 1.7 GHz $\pm$ 400 MHz and a sufficient linearity for amplitude variation as well as for phase variation. A decision circuit is composed of a wide-band dc amplifier and a high-speed flip-flop. The decision of input signal polarity is made at the rising edge of a clock signal provided to the flip-flop. The ambiguous discrimination width of the decision circuit is 6 percent of the eye opening of the demodulated signal.

The circuit configuration of the analog multiplier is shown in Fig. 5. It is composed of three twin transistors of $f_T = 6$ GHz and a transistor for use as the current source. This circuit is fabricated on an alumina-ceramic substrate as a hybrid IC and provides a sufficient accuracy and stability for use as a multiplier of a 400-MHz operating speed.

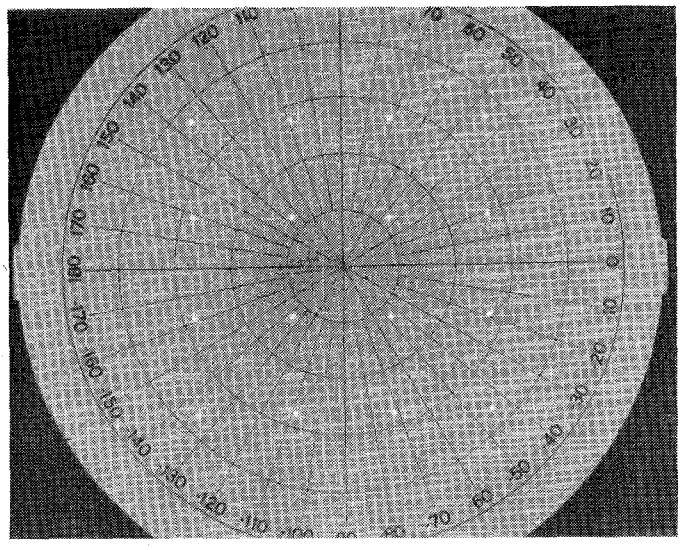

Fig. 4. Signal constellation of superposed APSK signal.

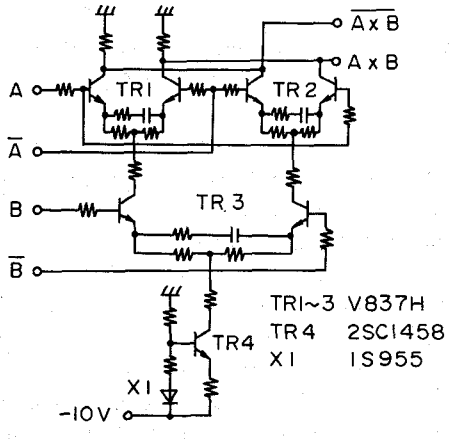

Fig. 5. Analog multiplier.

TABLE I
DESIGN PARAMETERS AND CHARACTERISTICS OF THE EXPERIMENTAL MODEM

CARRIER FREQUENCY	1700 MHz
CLOCK FREQUENCY	400 MHz
DATA RATE	1.6 Gb/S
REQUIRED CI/N FOR BER 1×10^{-9}	25.4 dB
CARRIER JITTER	-36 dB
LOOP GAIN	4.0×10^{8} Hz
NOISE BAND	1.5×10^{6} Hz
DAMPING FACTOR	0.7

The carrier recovery circuit uses the main loop mentioned in the preceding section and a subloop of an astatic control circuit so that the steady-state phase error due to the center frequency variation of the input carrier and free-running frequency variation of the voltage-controlled oscillator can be suppressed. The phase lock loop is designed to have loop parameters of a dc loop gain K of 4×10^{8} Hz, a noise bandwidth B_L of 1.5×10^{6} Hz, and a damping factor ξ of 0.7.

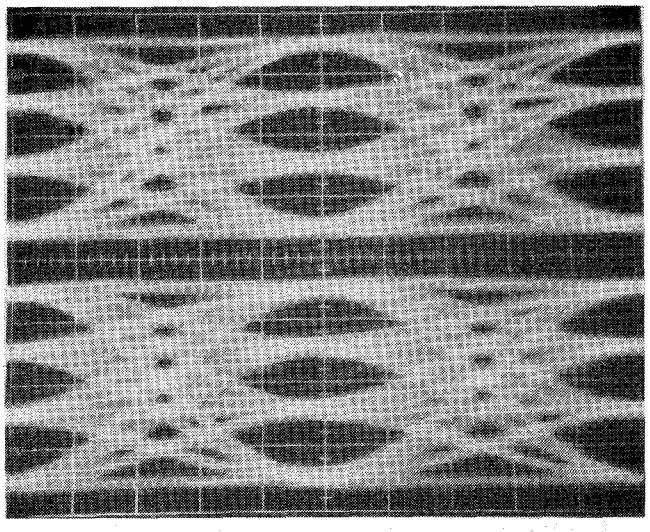

Fig. 6. Eye diagrams of the demodulated signals ($S_1(t)$ and $S_2(t)$ in Fig. 2). H: 0.5 nS/div.

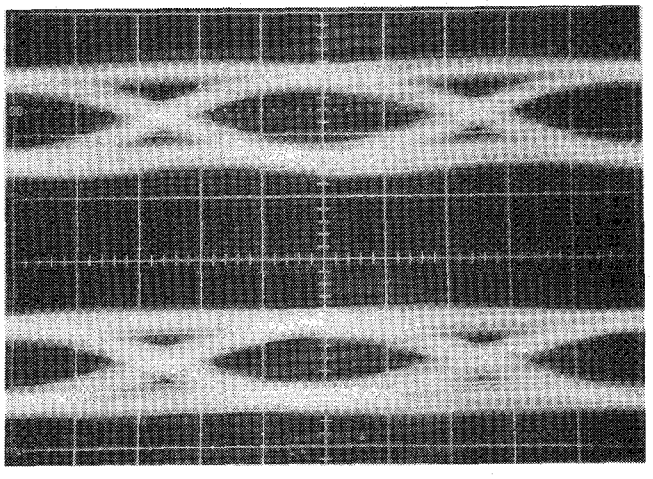

Fig. 7. Eye diagrams of the first-stage quantizing error signals ($S_1'(t)$ and $S_2'(t)$ in Fig. 2). H: 0.5 nS/div.

C. Characteristics of the Demodulation System

The modulating data signals for the modem loop-back test are 11- and 15-stage maximum-length pseudorandom sequences. To simulate the transmission path, a 5-stage Thomson bandpass filter ($BT=1.35$) is employed.

Fig. 6 shows the eye diagrams of the demodulated signals which correspond to $s_1(t)$ and $s_2(t)$ in Fig. 2, respectively. Fig. 7 shows the eye diagrams of the first-stage quantizing error signals which correspond to $S_1'(t)$ and $S_2'(t)$ in Fig. 2, respectively.

The equivalent phase comparator characteristic of the carrier recovery loop is shown in Fig. 8. This figure shows there is no undesired stable point in the neighborhood of $\pm21°$ as anticipated in the preceding section. No false lock phenomenon is observed as expected.

The power spectrum of the recovered carrier is shown in Fig. 9. It is to be noted that the noise power is extremely small. The measured noise power is less than -36 dB below the recovered carrier power. This provides

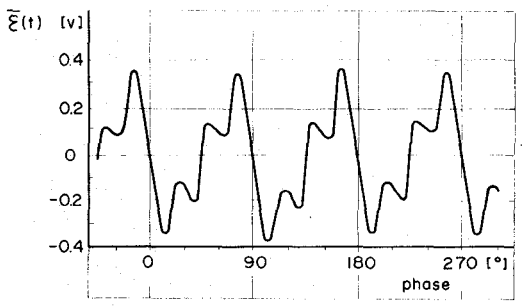

Fig. 8. Measured equivalent phase detector characteristic.

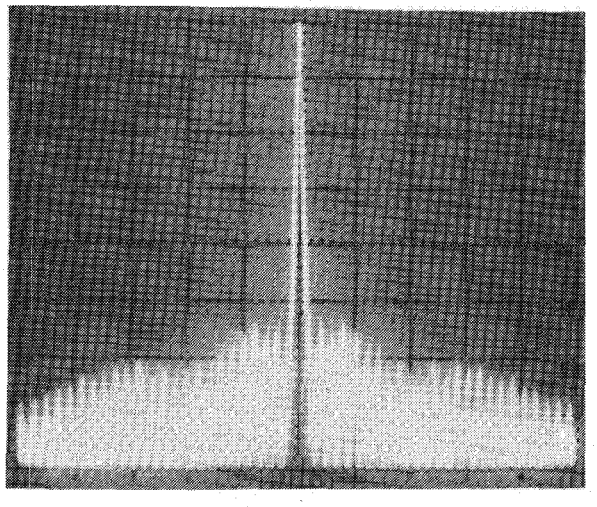

Fig. 9. Power spectrum of recovered reference carrier. V: 10 dB/div; H: 1 MHz/div; IF 30 kHz.

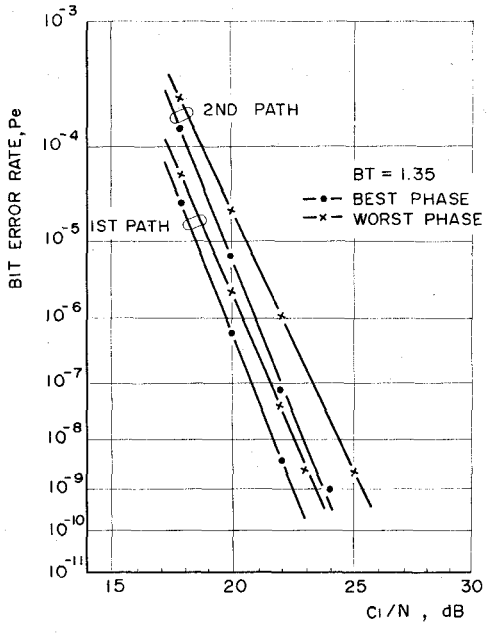

Fig. 10. Bit-error-rate characteristics, where C_1 denotes unmodulated carrier power of the first-path signal.

an excellent result as examined theoretically in the preceding section.

Fig. 10 shows the bit-error-rate characteristic obtained by the loop-back test of the modem. There are four possible pull-in phases corresponding to the equivalent

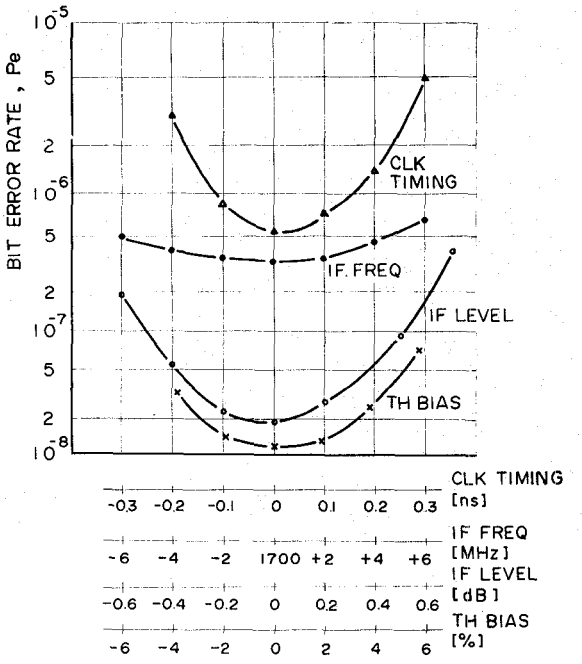

Fig. 11. Bit-error-rate variation due to parameter changes, where TH bias [%] denotes the ratio of decision threshold bias deviation to peak-to-peak signal level.

phase comparator characteristics and the bit-error-rate changes according to the pull-in phase. In this figure, the best and worst case data are shown for each first- and second-path regenerated data signal. The worst values of C_1/N for the bit error rate of 1×10^{-9} are 23.4 dB for the first path and 25.4 dB for the second path (C_1 is the unmodulated carrier power of the first-path signal). The worst degradation is about 3.8 dB relative to the theoretical limit for $BT=\infty$. Further improvement in the bit-error-rate characteristic will be achievable by improving impedance matching between circuits.

The performance characteristic degradation due to the incompleteness of the transmission path and modem circuits is a very important point for the modem design. The degradations due to some incomplete properties are measured by using this modem, and the results are shown in Fig. 11. It is required, to keep the bit-error-rate degradation less than twice as much as the value shown in Fig. 10, that the input signal level variation of the demodulator, the phase error of the clock signal for data signal regeneration, and the threshold level variation of the decision circuit should be within ±0.2 dB, within $\pm10°$, and within 2 percent of the peak value of the demodulated signal, respectively.

IV. Conclusion

The principles of operation and theoretical analysis of the performance of a 16-level superposed APSK modem based on a new operating principle are described. The circuit configuration and performance characteristics of 1.6-Gb/s 16-level APSK modem implemented on trial are presented. It has been verified theoretically and experimentally with this modem that carrier recovery is achievable with an extremely small pattern jitter, that there is no

false lock phenomenon, and that high-speed high-accuracy demodulation is achievable by a simple configuration. The influences of some degradation factors to bit-error-rate characteristics are studied experimentally, and their design objectives are stated.

Acknowledgment

The authors wish to thank Dr. H. Kimura, Dr. S. Seki, H. Ishio, and Dr. M. Akaike of the Electrical Communication Laboratories of NTT, and T. Kuroda and Dr. M. Sugiyama of the Nippon Electric Company, Ltd., for their helpful discussions and encouragement.

References

[1] C. R. Cahn, "Combined digital phase and amplitude modulation communication systems," *IRE Trans. Commun. Syst.*, vol. CS-8, pp. 150–155, Sept. 1960.
[2] J. C. Hancock and R. W. Lucky, "Performance of combined amplitude and phase-modulated communication systems," *IRE Trans. Commun. Syst.*, vol. CS-8, pp. 232–237, Dec. 1960.
[3] K. Miyauchi *et al.*, "A new technique for generating and detecting multi-level signal formats," *IEEE Trans. Commun. Technol.*, vol. COM-24, pp. 263–267, Feb. 1976.
[4] M. Washino *et al.*, "Experimental study on a new 1.6-GBps 16-level APSK modem," *NTC* '77, pp. 05:6–1, 05:6–6, Nov. 1977.
[5] M. K. Simon and J. G. Smith, "Carrier synchronization and detection of QASK signal sets," *IEEE Trans. Commun. Technol.*, vol. COM-22, pp. 98–106, Feb. 1974.
[6] H. Kobayashi, "Simultaneous adaptive estimation and decision algorithm for carrier modulated data transmission systems," *IEEE Trans. Commun. Technol.*, vol. COM-19, pp. 268–280, June 1971.
[7] F. D. Natali and W. J. Walbesser, "Phase-lock-loop detection of binary PSK signals utilizing decision feedback," *IEEE Trans. Aerosp. Electron. Syst.*, AES-5, pp. 83–90, Jan. 1969.
[8] T. Shimamura *et al.*, "400-MB QPSK repeater using a modified costas carrier tracking loop for millimetric waveguide transmission systems," in *Inst. Elec. Eng. Conf. Publ.* no. 146. *Millimetric Waveguide System*, Nov. 1976, pp. 163–166.
[9] M. Inokuchi *et al.*, "Experiments on the 1.6-Gb/s 16-level superposed modulation modem circuits," *IECE*, vol. 60-B, no. 8, (Japanese), pp. 598–600, Aug. 1977.

Calibrating the Six-Port Reflectometer by Means of Sliding Terminations

GLENN F. ENGEN, SENIOR MEMBER, IEEE

Abstract—**The six-port technique promises to have a major impact on the next generation of automatic network analyzers because complex heterodyne methods may be replaced by simple amplitude detectors. This projection, however, is predicated upon the existence or development of calibration techniques which permit one to conveniently and accurately obtain the parameters which characterize the six-port. This paper describes a number of substantial refinements to a previously described procedure which is based upon the use of sliding terminations.**

I. Introduction

THE APPEAL OF the six-port measurement concept stems largely from the simplification which it affords in the associated detection circuitry. Instead of complex heterodyne schemes, simple diode, thermoelectric, or bolometric detectors may be used. Because frequency conversion and mixing have been eliminated, practical experience, to date at least, indicates that a high order of stability in the source frequency, e.g., a frequency synthesizer, is not essential (although it certainly may be useful). Because of these simplifications, the six-port technique promises to have a major impact upon the next generation of automatic network analyzers. Morever, recent theoretical work has yielded an improved physical insight into the method so that it may now be applied with greater confidence [1].

The projected applications, however, are contingent upon the existence or development of appropriate calibration techniques which permit one to conveniently and accurately obtain the parameters which characterize the six-port. Although the calibration task does not pose any problems of a fundamental character, the supplementary requirements for convenience and speed (while not sacrificing accuracy), together with the general constraints imposed by an automated environment, combine to form the major challenge associated with the method.

As contrasted with the four-port reflectometer (which provides the basis for the existing network analyzers), the six-port reflectometer requires eleven rather than six constants for its calibration. Given this information, one might anticipate that the number of required terminations or standards and thus operator and computational effort would perhaps also be doubled. While this is nominally true of the computational effort, the procedures can still be handled by a desk-top programmable calculator.

Fortunately, this calibration scheme, along with others that have been described [2], is only slightly more in-

Manuscript received May 29, 1978; revised July 31, 1978.
The author is with the Electromagnetic Technology Division, National Bureau of Standards, Boulder, CO 80302.